Applied Energy 143 (2015) 383–394

Contents lists available at ScienceDirect

Applied Energy

journal homepage: www.elsevier.com/locate/apenergy

Temperature-dependent thermal properties of solid/liquid phase change even-numbered *n*-alkanes: *n*-Hexadecane, *n*-octadecane and *n*-eicosane

C. Vélez, M. Khayet *, J.M. Ortiz de Zárate

Department of Applied Physics I, Faculty of physics, University Complutense of Madrid, Avda. Complutense s/n, Madrid 28040, Spain

HIGHLIGHTS

- Thermal properties of *n*-hexadecane, *n*-octadecane and *n*-eicosane used as PCM are reported.
- Thermal conductivity and thermal diffusivity were measured by the hot wire technique at different temperatures.
- A discontinuity in thermal conductivity and diffusivity was detected near the melting temperature.
- No literature data were found for the thermal diffusivity of the three *n*-alkanes considered in this study.
- The cumulative heat stored increases with the number of carbon in the *n*-alkane hydrocarbon chain.

GRAPHICAL ABSTRACT

Variation of the cumulative heat stored in *n*-hexadecane (C_{16}), *n*-heptadecane (C_{18}) and *n*-eicosane (C_{20}) as function of temperature.

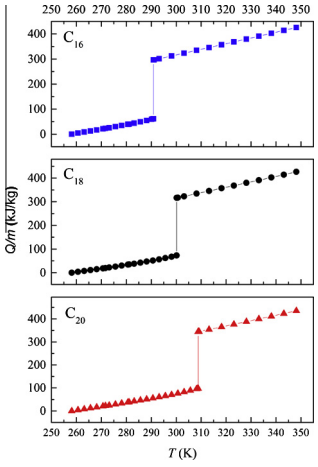

ARTICLE INFO

Article history:
Received 15 August 2014
Received in revised form 23 October 2014
Accepted 7 January 2015

Keywords:
n-Alkane
Phase change material
Energy storage
Thermal conductivity
Thermal diffusivity

ABSTRACT

The thermal conductivity (λ) and thermal diffusivity (a_T) of the solid/liquid phase change linear *n*-alkanes were measured simultaneously by the transient multi-current hot wire technique at atmospheric pressure in the range 258–348 K. The same set-up was used to measure λ and a_T of the liquid and the solid states at different electrical currents. Three *n*-alkanes, *n*-hexadecane ($C_{16}H_{34}$), *n*-octadecane ($C_{18}H_{38}$) and *n*-eicosane ($C_{20}H_{42}$) were studied. Differential scanning calorimetry was applied at the temperature range 248–348 K to determine the melting/crystallization temperature, the heat of melting/crystallization and the specific heat of both the solid and liquid phases. Some results were compared with available literature data. The density of the *n*-alkanes at liquid state was also measured at different temperatures and their thermal diffusivity was estimated and compared to that obtained by the hot wire technique. The cumulative energy stored was estimated over a definite range of temperature for the three *n*-alkanes and this was found to be higher for eicosane.

* Corresponding author. Tel.: +34 91 394 5185.
E-mail address: khayetm@fis.ucm.es (M. Khayet).

http://dx.doi.org/10.1016/j.apenergy.2015.01.054
0306-2619/

1. Introduction

Thermal energy can be stored as sensible heat, latent heat, thermo-chemical (i.e., heat involved in a reversible chemical reaction) or any combination between them. Among these methods, latent heat energy storage is particularly attractive due to its high-energy storage density (i.e., heat per unit volume) and to its ability to provide heat at a relatively constant temperature, which corresponds to the phase transition temperature of the used phase change material (PCM) [1–4].

In recent years, development of thermal energy storage systems using PCMs has gained a considerable importance in many applications such as in solar energy systems, in industrial waste heat and in energy-conserving buildings. PCMs can store from 5 to 14 times more heat per unit volume (i.e., storage density) than the sensible storage based materials such as water [2,5–8].

Among the four phase change possibilities (solid/gas, liquid/gas, solid/solid, and solid/liquid), solid/liquid transition is the most promising and economically attractive one for thermal energy storage systems. During melting cycle, energy is stored as latent heat of fusion, and then it is recovered during the solidification step. Compared to solid/gas and liquid/gas transitions, solid/liquid transition involves smaller change in volume (<10%) and therefore requires smaller space for storing although it involves, comparatively, smaller latent heat. On the other hand, in solid/solid transitions, heat is stored as a consequence of the crystalline change of the material and the involved latent heat as well as the volume change is less than those of solid/liquid transition. There are varieties of PCMs, both organic and inorganic, that melt and solidify at a wide range of temperatures and therefore are attractive in a number of applications [1,3,8–14]. A large number of solid/liquid PCMs have been studied for heating and cooling applications [7,9,15,16]. Therefore, for efficient heat recovery or energy storage design processes, it is necessary a good knowledge of the thermophysical properties of these PCMs in a wide range of temperature intervals.

The PCM should have suitable thermo-physical and chemical characteristics such as a phase-transition temperature in the desired operating temperature range, a high latent heat of transition per unit volume to allow a small size of the energy storage container, a high specific heat to provide additional sensible heat storage, a high thermal conductivity of both solid and liquid phases, a high density, a small volume change on phase transition, non-toxic, non-corrosive, non-flammable and not expensive. Except for the melting point in the desirable operating range, the majority of the used PCMs do not satisfy all these cited properties for an adequate storage system.

The inorganic PCMs exhibit generally a volumetric latent thermal energy storage capacity higher than that of organic PCMs. However, the organic PCMs melt congruently, have self-nucleation and are non-corrosive of the materials of construction. Paraffin waxes and linear *n*-alkanes (with the chemical formula C_nH_{2n+2}) belong to the latter group of PCMs and have some attractive features for solar energy systems [17]. It must be clarified that linear *n*-alkanes with number of carbons between 12 and 40 are known as paraffins. The *n*-alkanes have a large range of latent heats, various melting points, densities and specific heats [17]. However, an undesirable characteristic of *n*-alkanes is their low λ values, which may diminish the rate of the charging and discharging of the energy storage during the melting and solidification cycles. In general, for PCMs the higher λ the more efficient is the rate of heat transfer. Different possibilities have been adopted in order to compensate for the low λ values such as the use of finned configurations, containers and heat exchangers with adequate and improved designs to ensure efficient extraction and storage of heat, PCM encapsulation in different geometries, formation of composite by dispersing high-conductivity particles of different sizes and shapes, embedding metal matrix structures into PCMs, etc. [1,6,11,12,14,18–21].

Specific heat of *n*-alkanes has been thoroughly investigated using differential scanning calorimetry (DSC) by different research groups [22–24]. Comparatively, few research studies have been carried out on λ measurements of liquid *n*-alkanes [25–36] and solid *n*-alkanes but most of them were carried out near the solid/liquid phase transition temperature [26,37–41]. The thermal diffusivity (a_T) of *n*-alkanes including both solid and liquid phases has not yet been systematically studied by the hot wire technique. The reported data so far are for *n*-tricosane ($C_{23}H_{48}$), *n*-tetracosane ($C_{24}H_{50}$) and *n*-pentacosane ($C_{25}H_{52}$), measured by Fourier Transform Temperature Wave Analysis (FT-TWA) [42,43] and for liquid *n*-alkanes (C_nH_{2n+2}; n = 5–10) by the transient hot wire technique [36]. Additionally, a_T was estimated for a commercial paraffin PCM from the measured thermal conductivity (λ), density (ρ) and specific heat (c_p) (i.e., $a_T = \lambda/(\rho c_p)$) [5,44,45]. Moreover, it must be pointed out that most of the available λ values of *n*-alkanes are rather old and were performed either for the solid or for the liquid phases and not for both solid and liquid phases including the phase transition region.

The present paper is intended to discuss the thermal characteristics of the even-numbered *n*-alkanes, *n*-hexadecane, *n*-octadecane and *n*-eicosane for applications as low-temperature phase change energy storage medium. These *n*-alkanes are named hereafter C_{16}, C_{18} and C_{20}, respectively. C_{16} is liquid at room temperature and atmospheric pressure, whereas C_{18} and C_{20} are waxy solids. The transient multi-current hot wire technique, accepted as the most precise and reliable method to measure λ of fluids over a wide range of temperatures and pressures [26–29], was used in this study for the first time for both λ and a_T measurements of solid and liquid phases of PCMs. The melting/crystallization temperature, the heat of melting/crystallization and the specific heat of both the solid and liquid phases were determined by DSC.

2. Experimental

2.1. Materials

The used *n*-alkanes samples, *n*-hexadecane ($C_{16}H_{34}$), *n*-octadecane ($C_{18}H_{38}$) and *n*-eicosane ($C_{20}H_{42}$) having minimum purities of 99% were supplied by Sigma–Aldrich. The samples were used without any further purification or removal of dissolved water or air and no information was provided regarding the nature of the impurities. To check the adequate λ measurements of the wire, distilled water and dimethyl phthalate (99% purity, Sigma–Aldrich) with known λ values were used. Ethylene glycol (Fluka, 99.5%) was used as a thermostatic liquid. Methanol (99.8% purity, Sigma–Aldrich) and distilled water were used for calibration of the densimeter.

2.2. Measurements

The density of the *n*-alkane hydrocarbons was measured at different temperatures in liquid phase with a densimeter (Ludwig Schneider) having an accuracy of 1% and with an Anton Paar DMA 58 having a precision of ±0.05 kg/m^3.

Temperature variation test of the samples with time was carried out using a glass tube placed inside a thermostatic bath (Lauda ECO RE630) with a graduated heating and cooling option. For these experiments the applied heating/cooling rate was set to 0.2 °C/min. The sample was first melted, if not liquid at room temperature, and

then it was introduced in the glass tube having an internal diameter of 4 cm and a height of 32 cm. The volume of the samples was maintained the same (350 ml). A calibrated platinum resistance thermometer (F250-MK2 Precision thermometer, Automatic Systems Laboratories LTD) was placed inside the glass tube containing the sample. The platinum thermometer was interfaced to a computer having a written code that permits to register the temperature each 4 min and control the experiment. These tests permit to localize the phase change temperatures and compare their corresponding time.

The melting (T_m) and crystallization (T_c) temperatures of the samples together with their corresponding latent heats (ΔH_m and ΔH_c) were measured using differential scanning calorimetry (DSC1 instrument, Mettler Toledo) equipped with the software STARe for thermal data analysis. Indium was used as standard reference for the calibration of the instrument and the samples (7–9 mg) were sealed in aluminum pans. The tests were carried out in the temperature range 248–348 K at a heating rate of 2 °C/min and under a constant nitrogen flow rate at atmospheric pressure. The specific heat (c_p) of both the solid and liquid samples was determined for each *n*-alkane by DSC performed under a heating/cooling rate of 5 °C/min using the following expression:

$$c_p = \frac{HF}{mv} \tag{1}$$

where *HF* is the heat flow, v is the used scanning speed and m is the weight of the sample.

As it was indicated previously, λ and a_T were measured using the transient hot wire method. The experimental set-up shown in Fig. 1 and the method employed are essentially similar to the ones used in our laboratory for the measurement of λ of several fluids [25–27]. Since the details of the experimental set-up and the principles of measurements have been described elsewhere [25–27], only some minor changes will be noted. A vertical straight platinum wire of 50 ± 0.001 μm diameter and 20.13 ± 0.01 cm length was used. The two wire ends were soldered to tabs in a chemically resistant flat frame cut from a circuit board. Two Teflon isolated leads were then soldered to the tabs, after which the connections were covered by a thermal resistant epoxy. To avoid electrical contact between the platinum wire and the samples, the wire and the frame supporting it were covered with a Teflon-based industrial coating with a thickness less than 1 μm. A Keithley 2400 source-meter, which can act simultaneously as current source and voltage meter, was employed for electrical measurements. This source-meter is interfaced to a personal computer and a software code was written to retrieve the measurement points, fit the data, and then calculate λ and a_T. The electrical current is injected by two of the leads connected to the wire ends, while voltage measurements are acquired simultaneously using the other two leads. For each λ and a_T measurement, various current values, from 160 to 260 mA, were applied.

The *n*-alkane sample is first melted, if not liquid at room temperature, and poured in the inner volume of a double-wall cylindrical glass cell having an internal diameter of 4 cm, an external diameter of 6 cm and a height of 32 cm. Both the hot wire and the platinum resistance thermometer are inserted inside the cell containing the *n*-alkane sample. The platinum thermometer is also interfaced to the personal computer controlling the experiment, and the same computer code manages simultaneously the thermometer and the electrical source-meter. Ethylene glycol is circulated from a thermostated bath (Lauda ECO RE630) through the jacket of the measurement glass cell in order to control the temperature of the sample within ±0.05 K. The whole measurement cell is placed inside a controlled laboratory environmental chamber (Mytron) that is set at the same temperature of the thermostat. The humidity of the chamber was maintained around 40%.

To ensure the adequate measurements of the wire, series of experimental runs using distilled water and dimethyl phthalate at different temperatures were performed at the beginning and at the end of each experiment as well as when switching between the different *n*-alkanes. Comparisons with known values of λ for distilled water and dimethyl phthalate were made.

At the first beginning of the experiment, the temperature is established. Once steady state is reached, by means of the developed software the electrical current was varied within the established range with a difference of 20 mA, which is applied to the wire every 4 min. The resistance of the wire (R_0) at the beginning of the heating step, the electric potential (V) and the temperature

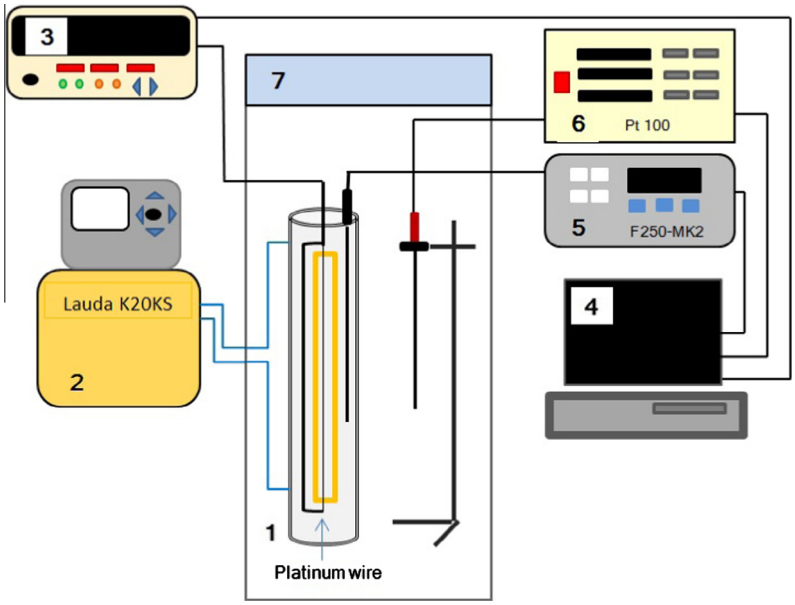

Fig. 1. Schematic representation of the experimental set-up for the measurement of the thermal conductivity (λ) and thermal diffusivity (a_T). (1) Measurement cell, (2) Lauda K20KS thermostatic circulation bath, (3) Keithley 2400 Source Meter, (4) computer, (5) ASL F250 reference thermometer, (6) Pt 100 digital thermometer for monitoring chamber temperature, and (7) atmospheric chamber with controlled temperature and humidity (Mytron).

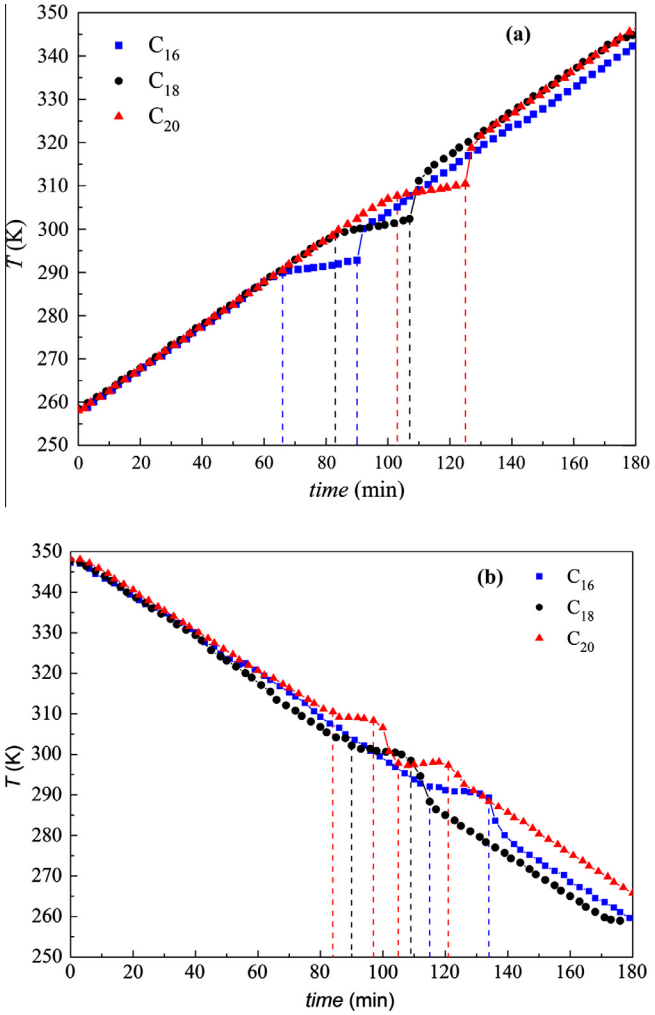

Fig. 2. Melting temperature curves (a) solidification temperature curves and (b) of the three even-numbered *n*-alkanes (C_{16}, C_{18} and C_{20}). Dotted lines represent the melting temperature range.

(T) versus time (t) are recorded. En each measurement 350 values of V as a function of time are registered. Each temperature measurement is performed for at least 10–12 h depending on the set temperature and the state of the *n*-alkane hydrocarbon, solid or liquid, under study. A typical heating run lasts for approximately 1.6 s.

When the electrical current I is circulated through the wire, because of Joule heating, the wire temperature increases. The rate of wire heating depends mainly on λ and a_T of the *n*-alkane surrounding the wire. As a consequence of the temperature increase, both the electrical resistance of the wire (R) and the voltage drop between the wire ends ΔV increase. For an infinite cylindrical straight wire, ΔV between two points, separated by a distance L, as a function of time t, can be approximated for large time, $t \gg \frac{r_0^2 \rho c_p}{4\lambda}$, by Refs. [27,28,46]:

$$\Delta V(t) = V(t) - V_0 = \alpha \frac{I^3 R_0^2}{4\pi\lambda L}\left[\ln\left(\frac{4\lambda t}{r_0^2 \rho c_p}\right) - \gamma\right] \quad (2)$$

where R_0 is the electrical resistance of the wire at the beginning of the heating ($t = 0$), γ is Euler's constant ($\gamma = 0.5772$), α is the temperature resistance coefficient of the wire material (Platinum) and L is the wire length. This equation can be re-written as:

$$V(t) = m \frac{I^3 R_0}{4\pi\lambda L}\left[\ln\left(\frac{t}{\beta}\right) - \gamma\right] + V_0 \quad (3)$$

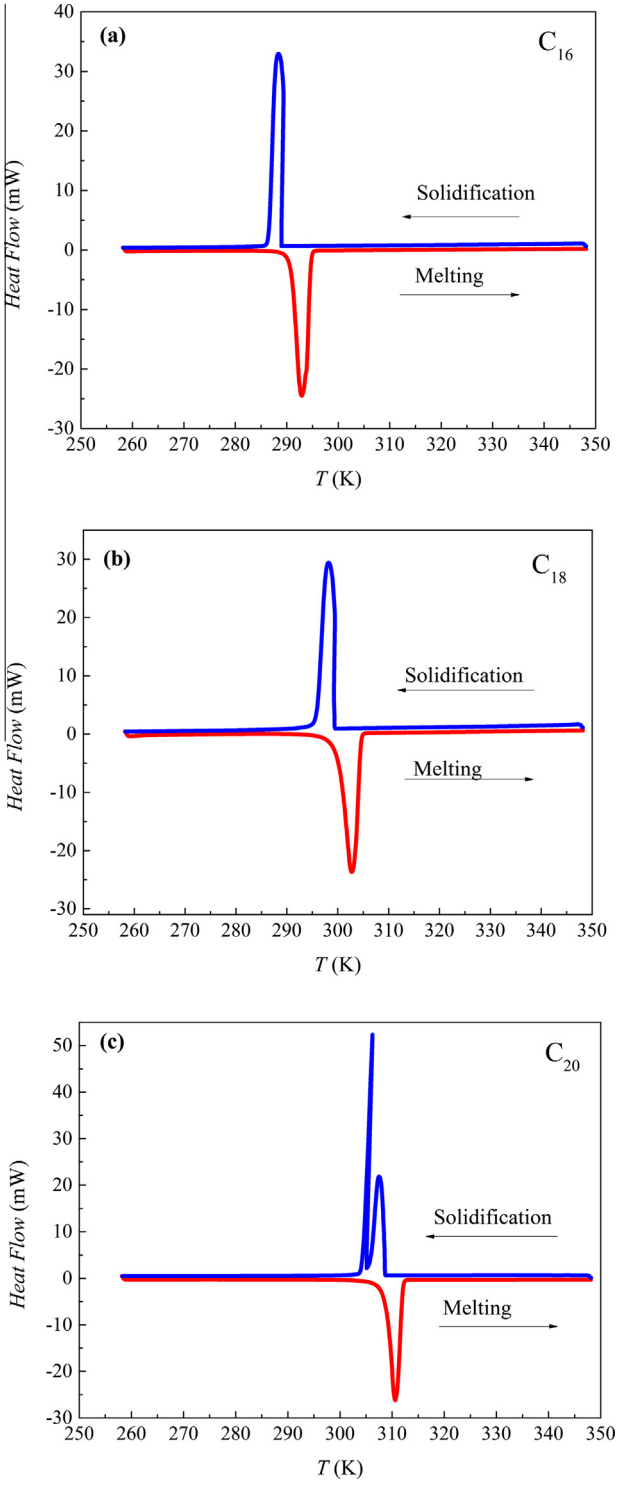

Fig. 3. Differential scanning calorimetry (DSC) thermograms of: (a) C_{16}, (b) C_{18} and (c) C_{20}.

where ($m = \alpha R_0$) represents the slope of the {R, T} curve at the initial temperature of the heating run and the parameter β (units of time) depends on a_T of the sample and the wire radius (r_0) as follows:

$$\beta = \frac{r_0^2}{4a_T} \quad (4)$$

λ of the sample is obtained by fitting, as required by Eq. (3), the data pairs {V_i, ln(t_i)} acquired in each heating run to a straight line, from

Table 1
Melting temperature (T_m), heat of melting (ΔH_m), crystallization temperature (T_c), solid/solid transition temperature (T_r) and heat of crystallization (ΔH_c) of C_{16}, C_{18} and C_{20} determined from DSC thermograms presented in Fig. 3.

n-Alkane	Melting		Crystallization		
	Solid/liquid transition		Liquid/solid transition	Solid/solid transition	
	T_m (K)	ΔH_m (kJ/kg)	T_c (K)	T_r (K)	ΔH_c (J/g)[a]
C_{16}	290.90 ± 0.006	235.13 ± 0.13	289.96 ± 0.16	–	236.89 ± 0.20
C_{18}	300.22 ± 0.095	243.68 ± 0.096	300.87 ± 0.10	–	244.53 ± 0.14
C_{20}	308.84 ± 0.15	247.05 ± 0.14	309.27 ± 0.001	305.42 ± 0.10	248.33 ± 0.18

[a] For C_{20} the indicated latent heat is the total considering both solid/solid and solid/liquid phase changes.

which a slope (S) and intercept (B) are derived. Since Eq. (3) is an asymptotic expansion for large t, only the points acquired after ≈412 ms were used in the fitting procedure. Finally, λ and a_T can be determined from the following expressions:

$$\lambda = \frac{mI^3R_0}{4\pi LS} = A\frac{I^3R_0}{S} \tag{5}$$

$$a_T = \frac{r_0^2}{4}\exp\left(\frac{B - V_0}{S} + \gamma\right) \tag{6}$$

where A is a constant of the wire that depends on its effective length.

3. Results and discussions

Fig. 2 shows the melting and crystallization temperatures variation curves with time of the three *n*-alkanes. The melting time was estimated from the temperature curves as the time corresponding to a constant temperature of the *n*-alkane. This is 24 min, 24 min and 22 min, for C_{16}, C_{18} and C_{20}, respectively. The detected melting temperature range is (289.91–292.78 K), (298.67–302.35 K) and (307.68–310.45 K) for C_{16}, C_{18} and C_{20}, respectively. It must be pointed out that the reduction of the melting time corresponds to the higher λ value of the *n*-alkane or to the greater latent heat of melting and mass. Similar to the melting curve, from the solidification curve the corresponding temperature range and solidification time were determined for each *n*-alkane. The estimated crystallization time was 19 min for C_{16} and C_{18}, whereas for C_{20} it was lower, 16 min and 13 min for liquid/solid transition and solid/solid transition, respectively. The crystallization temperature range was (292.05–289.30 K) for C_{16} and (298.43–302.16 K) for C_{18}; while for C_{20} it was (308.33–310.49 K) and (297.29–298.81 K) for liquid/solid and solid/solid transitions, respectively.

Fig. 3 shows the DSC curves of the three *n*-alkanes. From the quantitative analysis of the DSC thermograms, the melting temperature (T_m), the crystallization temperature (T_c), the solid/solid transition temperature (T_r) of C_{20}, the heat of melting (ΔH_m) and the heat of crystallization (ΔH_c) were determined. The results of three DSC essays for each *n*-alkane are summarized in Table 1. It can be seen in Fig. 3 that the DSC thermograms of C_{16} and C_{18} have a single peak both for heating (i.e., melting) and cooling (i.e., crystallization), whereas C_{20} exhibits other than a single endothermic absorption melting peak, two almost overlapping crystallization peaks. The minor peak represents the liquid/solid phase change (i.e., crystallization) while the large peak (called secondary peak) represents the solid/solid transition indicating the structural phase change in the solid [28]. It must be pointed out that the presence of two peaks for C_{20} is characteristic of odd-numbered *n*-alkanes and hydrocarbons with carbon number greater or equal to 19 (i.e., *n*-nonadecane, $C_{19}H_{40}$). Triclinic structure (i.e., crystalline I) has been confirmed by X-ray Diffraction (XRD) at lower temperatures than T_r while rotator crystal was reported for higher temperatures up to T_m [47,48].

For all *n*-alkanes, the temperatures T_m and T_c determined from DSC curves by means of STAR^e software are found to be within the temperature ranges obtained from Fig. 2, except for the solid/solid transition temperature of C_{20}. From DSC analysis this is 305.42 K, whereas the temperature range shown in Fig. 2 is slightly lower (297.29–298.81 K). As it was claimed by Genovese et al. [24], this result may be attributed to the different solidification rates applied that were 2 °C/min in DSC and 0.2 °C/min in the thermostatic bath used to obtain the crystallization temperature curve. In addition, the discrepancy between the DSC and the temperature curves based values may be attributed to the amount of *n*-alkane used in the experimental test 7–9 mg for DSC and about 272 g (350 ml) for temperature variation tests. The thermal stability of a small amount is much better than for a large amount of sample.

It was observed a gradual increase of ΔH_m, ΔH_c, T_m and T_c with increasing the number of carbon atoms of the *n*-alkane (see Table 1). Table 2 summarizes some T_m and ΔH_m reported values in other studies, which are found to be very close to the obtained ones in this study for the three *n*-alkane hydrocarbons (i.e., the deviations were less than 0.8%), except the data reported by Jiang et al. [51], which showed greater deviations 4.2% and 1.2% for ΔH_m and T_m, respectively. This may be attributed to the higher heating rate used (i.e., 10 °C/min). It must be mentioned that, in general, the three *n*-alkanes exhibit a satisfying latent heat capacity for latent heat thermal energy storage systems applications.

It is worth noting that T_c of C_{20} obtained by Genovese et al. [24], 308.75 K, is quite similar to that obtained in this study, whereas the T_r value reported by Genovese et al. [24] as initial solid/solid phase change temperature is 307.15 K, which is 0.6% greater than that obtained in this study. In Fig. 3(c) it can be seen the quick exothermic solid/solid phase change resulting in a slightly declined peak to higher temperature, which corresponds to an initial

Table 2
Reported melting temperature (T_m) and heat of melting (ΔH_m) of C_{16}, C_{18} and C_{20}.

n-Alkane	T_m (K)	ΔH_m (kJ/kg)	Reference[a]
C_{16}	291.25	236	[17]
	289.85	236	[23]
	291.49	235.65	[49]
	291.15	237	[50]
C_{18}	301.25	244	[17]
	301.6	242.48	[49]
	301.15	243	[50]
C_{20}	309.75	248	[17]
	310.3 ± 0.1	247.6 ± 0.2	[24]
	310.05	247.6	[49]
	310.15	247	[50]
	312.3	237.1	[51]

[a] The data reported in [23,24] were obtained from DSC analysis while the other reported data in [17,49–51] no specific technique was mentioned. T_c and ΔH_c values of C_{16} and C_{18} were not found. The only available T_c and ΔH_c values are for of C_{20} and these were reported by Genovese et al. [24] and indicated in the text of this study.

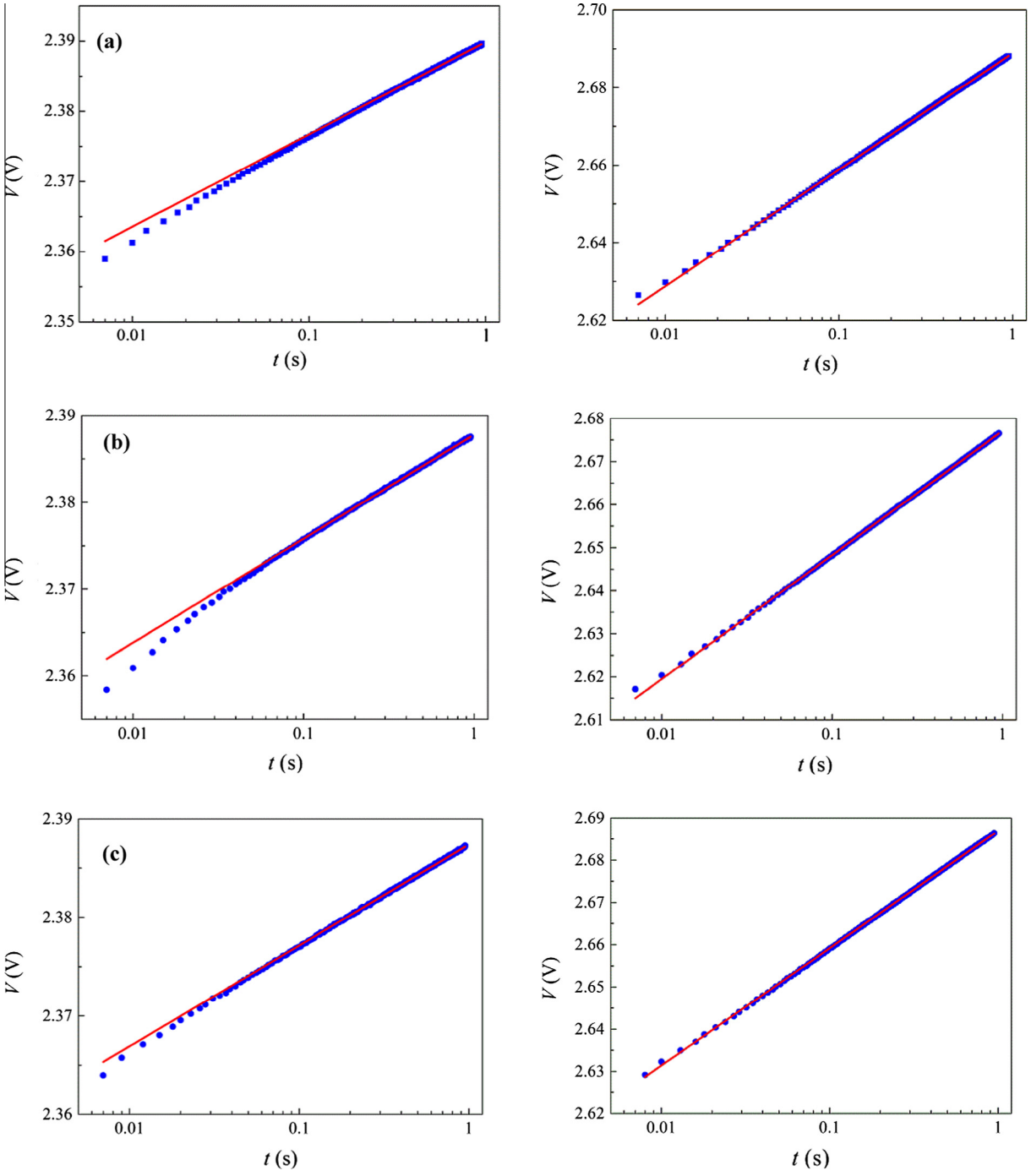

Fig. 4. Examples of heating curves of the plantinum wire presenting the electric voltage between the ends of the wire as a function of time at 10 °C (left, solid phase) and 40 °C (right, liquid phase) for: (a) C_{16}, (b) C_{18} and (c) C_{20}. The intensity used in these measurements is $I = 200$ mA.

solid/solid phase change temperature of 306.23 K. This result is attributed to the heat evolved in the solid/solid conversion [24].

Some examples of heating curves $\{V, \ln t\}$ used to determine λ of solid and liquid phases of the three n-alkanes are presented in Fig. 4. The solid lines represent the adjustment of the experimental points to Eq. (3) when the system reached asymptotic long times (i.e., $\gg$412 ms; The first 150 points have not been taken into account in the fitting). No deviations were observed between the registered data and the straight lines at long time asymptotic regime. This demonstrates that the measurements in liquid state are free of natural convection.

For each n-alkane sample, two series of measurements were performed, one from lower to higher temperature and the second from higher to lower temperature. R is registered for each sample both in solid or liquid phase, for each temperature and for each electrical current measurement. An average value is then determined and the dependence of R with temperature (T) is plotted in Fig. 5. The obtained m value is 0.04452 Ω/K. From the measured and reported λ values of water and dimethyl phthalate at different temperatures, A was determined (0.01783 $\Omega\,K^{-1}\,m^{-1}$) and then the effective length of the wire (L_{eff}) was calculated from Eq. (5) ($L_{eff} = m/(4\pi A)$). The obtained value 19.87 cm is close to the used length of the wire 20.13 cm (1.3% deviation). This confirms that the measured λ and a_T data in this study are absolute values. It is worth quoting that the behavior of the electrical resistance with temperature permits to check the stability of the wire during the

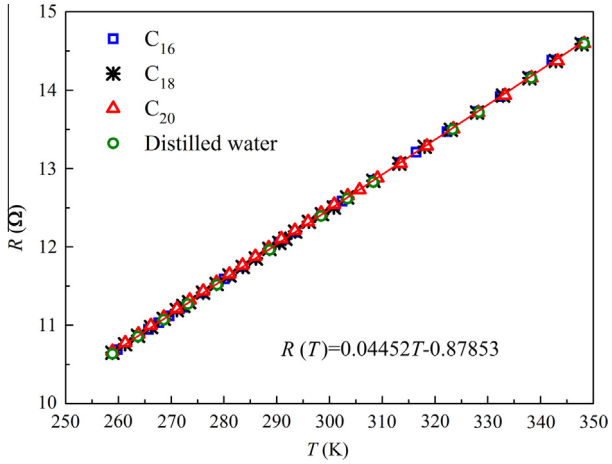

Fig. 5. Resistance (R) of the used platinum wire as a function of temperature (T) of C_{16}, C_{18}, C_{20} and distilled water used for calibration.

measurements period. Most importantly, no differences were detected between tests performed with water and dimethyl phthalate at the beginning, at the end and when switching between tested alkane hydrocarbons.

Fig. 6 shows λ of C_{16}, C_{18} and C_{20} in both liquid and solid phases as a function of temperature together with the available literature data [26,29–35,39–41]. The reported standard deviations correspond to 100–445 measurements of each temperature. The uncertainty indicated for λ values corresponds to random errors only and a systematic error contribution of ±2% should be added. This is considered in the supplementary Table summarizing λ data. For clarity, horizontal lines were plotted to separate the measurements carried out in each phase. High dispersions of λ were detected near the solid/liquid phase transition of the three n-alkanes. This is attributed to the latent heat of melting/crystallization that may affect the temperature of the wire. In any case, the error bars are between 0.6% and 2.2% for C_{16}, 0.10% and 4.5% for C_{18} and 0.3% and 1.2% for C_{20}. It can also be seen that the literature data [26,29–35,39–41] are within the margin of error in the liquid phase for C_{16} and C_{20}, while for the solid phase it is impossible to make any comparison due to the insufficient available data in the literature. For C_{18}, the obtained λ values in liquid phase are quite similar to those reported by Yaws [31] but higher than those given by Mustafaev [34] and Rastorguev and Bogatov [35]. As it is reported previously, there is a lack of published data for the solid phases of the three n-alkanes and all published λ values of the solid phase of n-alkane hydrocarbons correspond to temperatures very close to the transition temperature (T_m) without indication of the corresponding associated errors and these values are larger than λ obtained in this study [26,29–35,39–41].

It can be observed in Fig. 6 that in the liquid phase λ of the three n-alkanes tends to decrease with the increase of the temperature. However, for C_{16} and C_{20} in solid phase λ is maintained nearly constant for temperatures much lower than T_m and decreased gradually with temperatures near T_m. For C18 in solid phase, a more clear decrease of λ was detected with the increase of the temperature (Fig. 6b). A discontinuity in λ is detected near T_m of each n-alkane being λ of the same n-alkane in solid state higher than that of the liquid state and the jump of λ at the liquid/solid phase transition is higher for the n-alkane having higher number of carbon atoms. This is attributed principally to the change of the density, typical of first order phase transition. The estimated ($\Delta\lambda = \lambda_{solid} - \lambda_{liquid}$) is 0.172, 0.182 and 0.263 W/m K for C_{16}, C_{18} and C_{20}, respectively. Moreover, in solid phase λ is greater for the n-alkane having greater number of carbon in the molecular chain.

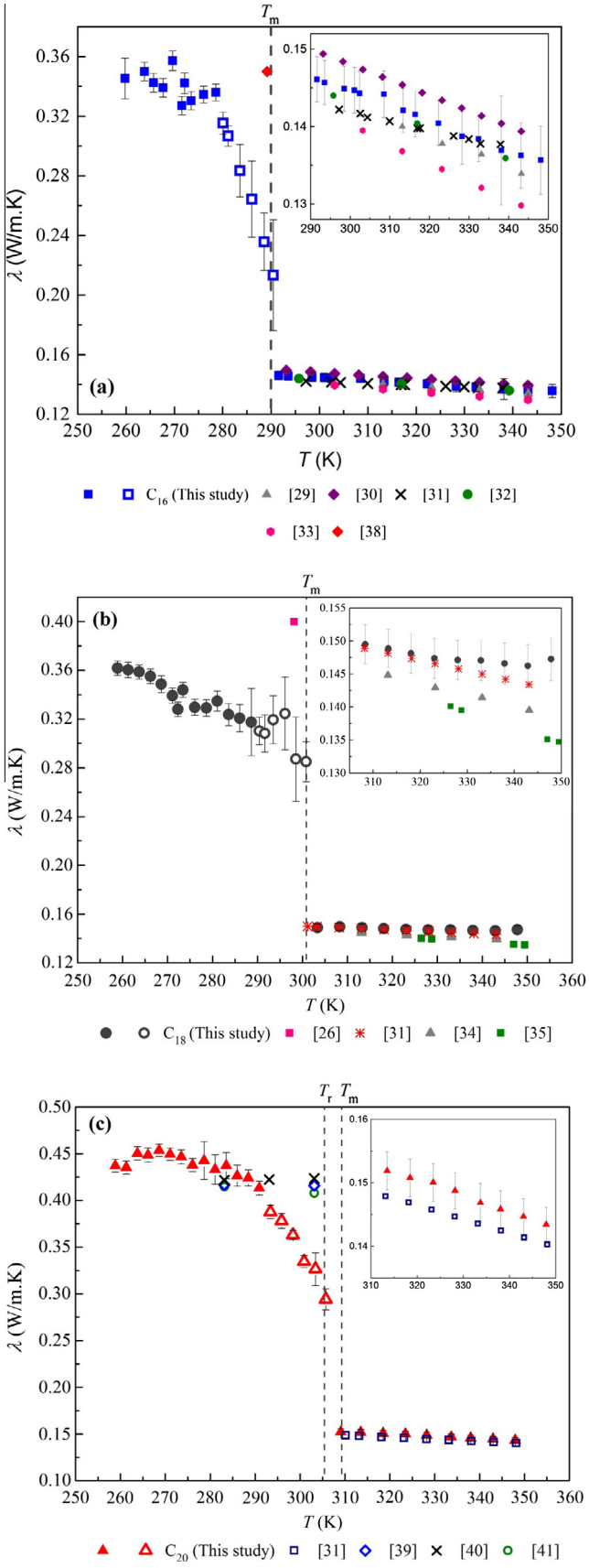

Fig. 6. Thermal conductivity (λ) of solid and liquid phases as a function of temperature (T) of: (a) C_{16}, (b) C_{18} and (c) C_{20}. The measured (λ) data in solid phase near the transition temperature (presented as empty symbols) are affected by the latent heat.

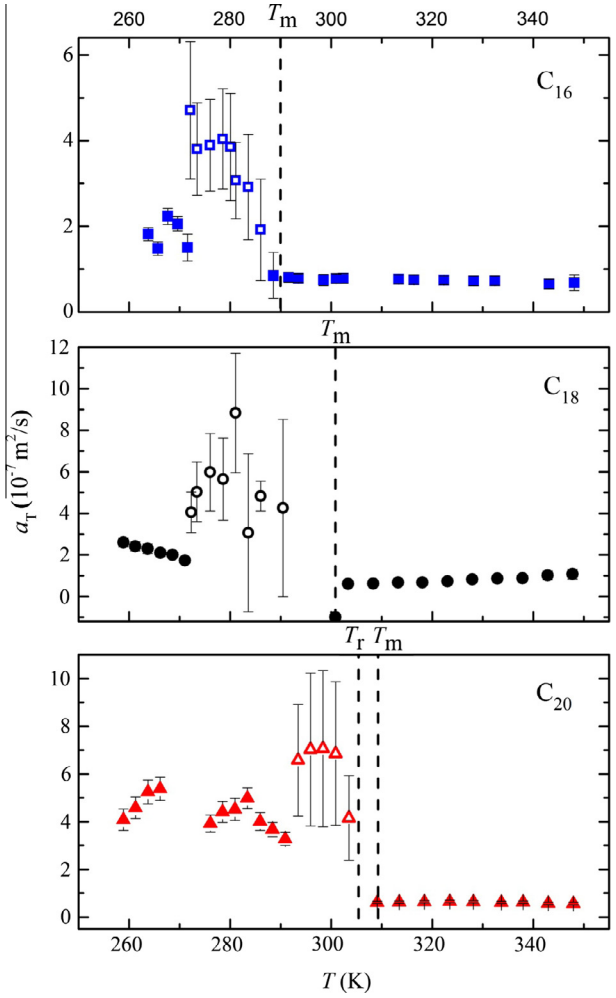

Fig. 7. Thermal diffusivity (a_T) of solid and liquid phases as a function of temperature (T) of: (a) C_{16}, (b) C_{18} and (c) C_{20}. The measured (a_T) data in solid phase near the transition temperature (presented as empty symbols) are affected by the latent heat.

Table 3
Some a_T data of C_{16}, C_{18} and C_{20} in liquid phase obtained by the hot wire technique and calculated ($a_T = \lambda/(\rho c_p)$) from the measured λ, ρ and c_p in this study.

n-Alkane	T (K)	a_T (10^{-7} m^2/s)	
		Measured by the hot-wire technique	Calculated $a_T = \lambda/(\rho c_p)$
C_{16}	291.58	0.81 ± 0.15	0.85 ± 0.18
	293.53	0.78 ± 0.14	0.85 ± 0.19
	298.49	0.75 ± 0.16	0.85 ± 0.18
	301.02	0.78 ± 0.14	0.85 ± 0.18
	302.39	0.78 ± 0.14	0.85 ± 0.18
	313.37	0.76 ± 0.14	0.84 ± 0.18
	316.41	0.75 ± 0.14	0.83 ± 0.18
	322.28	0.74 ± 0.13	0.82 ± 0.18
	328.26	0.72 ± 0.14	0.81 ± 0.18
	332.40	0.73 ± 0.14	0.81 ± 0.18
	343.14	0.65 ± 0.14	0.79 ± 0.18
	348.10	0.68 ± 0.22	0.78 ± 0.18
C_{18}	303.36	0.60 ± 0.06	0.85 ± 0.27
	308.318	0.62 ± 0.07	0.86 ± 0.17
	313.24	0.67 ± 0.07	0.86 ± 0.18
	318.05	0.68 ± 0.07	0.86 ± 0.18
	323.019	0.73 ± 0.12	0.85 ± 0.18
	327.96	0.83 ± 0.14	0.85 ± 0.17
	332.911	0.86 ± 0.16	0.84 ± 0.17
	337.92	0.88 ± 0.18	0.84 ± 0.17
	342.90	1.01 ± 0.25	0.83 ± 0.17
	347.81	1.07 ± 0.27	0.82 ± 0.17
C_{20}	309.10	0.61 ± 0.08	0.86 ± 0.12
	313.50	0.62 ± 0.08	0.86 ± 0.12
	318.48	0.63 ± 0.09	0.86 ± 0.12
	323.48	0.65 ± 0.09	0.85 ± 0.12
	328.20	0.63 ± 0.09	0.84 ± 0.12
	333.69	0.61 ± 0.09	0.83 ± 0.12
	338.04	0.62 ± 0.09	0.82 ± 0.12
	343.00	0.57 ± 0.09	0.81 ± 0.11
	347.94	0.56 ± 0.09	0.79 ± 0.11

In liquid phase, λ is also higher for the hydrocarbon with more number of carbon atoms in the molecular linear chain. A gradual decrease of λ is observed for C_{16} and C_{20} in all studied temperature range and for C_{18} from its melting temperature to 333.15 K. A constant value of λ was measured for C_{18} from 333.15 K to 348.15 K. For C_{20} no λ variation could be detected for the two crystalline phases because of the close T_m and T_r values.

The reported λ values for C_{16} in liquid phase [29,30] deviate only 2.5% from the values obtained in this study. For C_{18} and C_{20} in liquid phase the λ values obtained in this study are less than 2% and 2.9% higher than those reported by Yaws [31] and Stryker and Sparrow [39], respectively.

a_T was also determined by the hot wire technique for both the solid and liquid phases of the three *n*-alkanes as it was explained previously (Eq. (6)). The results are plotted in Fig. 7 and summarized in Table 3. The uncertainty indicated for a_T values in Fig. 7 corresponds to random errors only and a systematic error contribution of ±3.5% should be added. In Table 3, the total errors are indicated together with the obtained a_T values. It can be seen that the uncertainty associated to a_T obtained by the hot wire technique is greater than that of λ. For both liquid C_{16} and C_{20}, only very slight decrease was detected for a_T with temperature (i.e., 18.0% for C_{16} and 8.5% for C_{20} when the temperature was reduced to 348 K) and a_T of C_{20} is about 15% smaller than that of C_{16}. By means of the transient hot wire technique, Wanatabe and Seong [36] also observed a gradual decrease of a_T with the increase of the temperature from 263 K to 343 K of *n*-alkanes C_nH_{2n+2} (n = 5–10) and practically no difference was detected between a_T values of these studied *n*-alkanes that were maintained in the range 7–8.9 · 10^{-8} m^2/s. Wanatabe and Seong [36] claimed that a_T was maintained constant with the number of carbon atoms n of these *n*-alkanes and within the studied temperature range 263–343 K. Providing that Morikawa and Hashimoto [42] reported higher a_T values for the *n*-alkanes (*n*-tricosane ($C_{23}H_{48}$), *n*-tetracosane ($C_{24}H_{50}$) and *n*-pentacosane ($C_{25}H_{52}$)), it seems that there may be an increase of a_T with the number of carbon atoms n of linear alkanes.

It can be seen in Fig. 7, a slight enhancement of a_T with temperature for C_{18} in liquid phase. This result is attributed partly to the insignificant variation of λ with temperature from 318 to 348 K. It is interesting to note that, similar to λ in liquid phase up to 330 K, an increase of a_T with the number of carbon atoms of the *n*-alkanes was observed in the temperature range 310–325 K.

As it can be seen in Fig. 7, similar to λ, a_T of C_{16}, C_{18} and C_{20} in the solid phase is greater than that of the liquid phase and much dispersions were registered for a_T near T_m. Similar behaviors of a_T were reported by Morikawa and Hashimoto [42] for other *n*-alkanes (*n*-tricosane ($C_{23}H_{48}$), *n*-tetracosane ($C_{24}H_{50}$) and *n*-pentacosane ($C_{25}H_{52}$)) determined by means of Fourier Transform Temperature Wave Analysis (FT-TWA). It is worth quoting that no literature data were found for a_T of the three *n*-alkanes considered in this study.

a_T can be calculated using the obtained λ values in this study if c_p and ρ data are available. As it was mentioned previously, c_p of the three *n*-alkanes was determined from the DSC curves. The

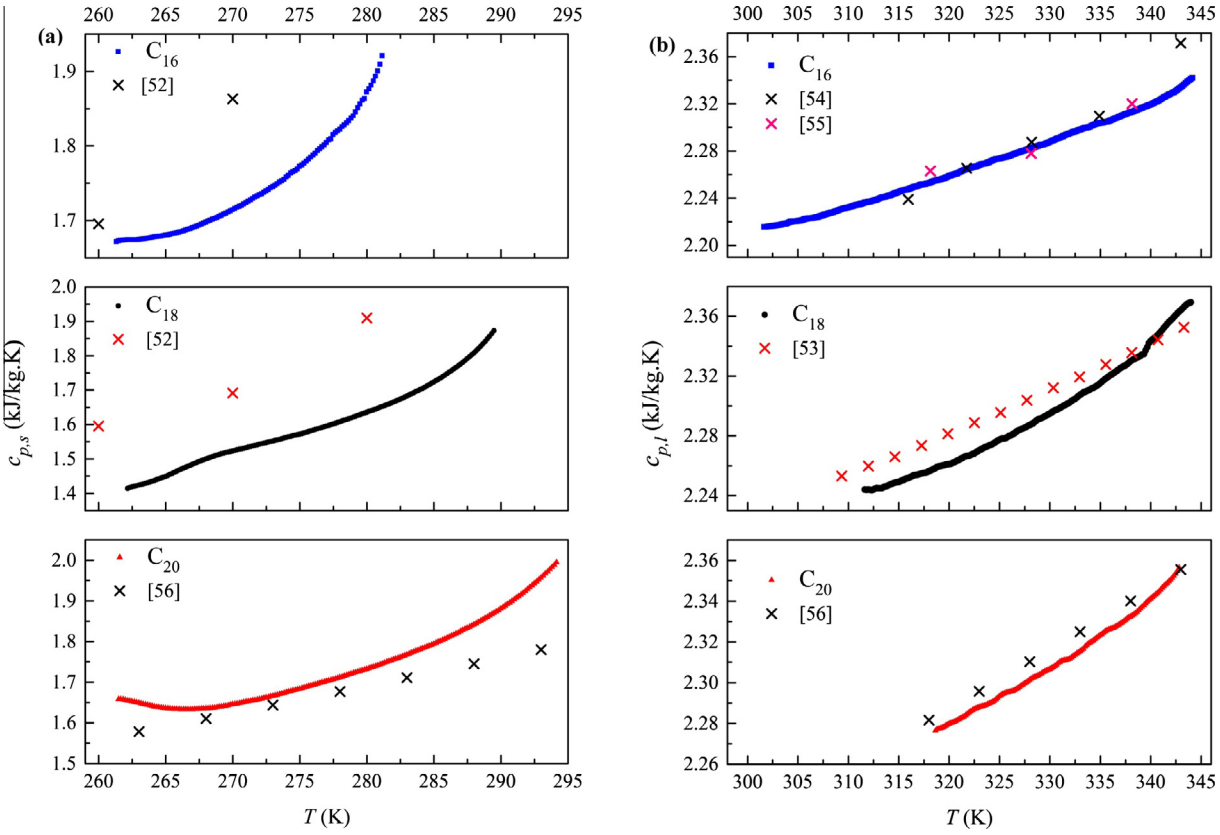

Fig. 8. Specific heat (c_p) of C_{16}, C_{18} and C_{20} as function of temperature. (a) Curves are for solid phase ($c_{p,s}$) and (b) curves are for liquid phase ($c_{p,l}$).

Table 4
Parameters a–e obtained from fitting c_p (in kJ/kg K) experimental data points to ($c_p = aT^4 + bT^3 + cT^2 + dT + e$) as a function of temperature T (in K) of n-alkane hydrocarbons in solid and liquid phases. With the reported parameters, the measured experimental data are represented within ±2%, that is around the estimated uncertainty of the data themselves.

n-Alkane	*a*	*b*	*c*	*d*	*e*
Solid					
C_{16}	$2.698 \cdot 10^{-6}$	$-2.909 \cdot 10^{-3}$	1.177	−211.566	$1.427 \cdot 10^{+4}$
C_{18}	$8.804 \cdot 10^{-7}$	$-9.390 \cdot 10^{-4}$	0.375	−66.573	$4.425 \cdot 10^{+3}$
C_{20}	$1.048 \cdot 10^{-6}$	$-1.165 \cdot 10^{-3}$	0.485	−89.957	$6.254 \cdot 10^{+3}$
Liquid					
C_{16}	$6.017 \cdot 10^{-8}$	$-7.778 \cdot 10^{-5}$	$3.770 \cdot 10^{-2}$	−8.118	657.233
C_{18}	$1.698 \cdot 10^{-7}$	$-2.229 \cdot 10^{-4}$	$1.098 \cdot 10^{-1}$	−24.026	$1.975 \cdot 10^{+3}$
C_{20}	$3.192 \cdot 10^{-7}$	$-4.188 \cdot 10^{-4}$	0.206	−45.041	$3.694 \cdot 10^{+3}$

results together with the reported data obtained from the literature [52–56] are presented in Fig. 8. There is an increase of c_p of the three *n*-alkanes with temperature in both solid and liquid phases.

The deviation between the obtained c_p data in this study for the three *n*-alkane hydrocarbons in liquid phase are less than 1.61%, 0.91% and 0.36% for C_{16}, C_{18}, C_{20}, respectively [53–56]. Greater deviation errors were found for the solid phase, which were 8.58%, 16.58% and 9.26% for C_{16}, C_{18}, C_{20}, respectively [52,56]. This may be attributed to the different used measurement techniques. For C_{16} and C_{18} an aneroid calorimeter was used [52] whereas for C_{20} an adiabatic calorimeter was employed [56]. Table 4 summarizes the fitting coefficients of c_p values to the polynomial equation ($c_p = aT^4 + bT^3 + cT^2 + dT + e$).

ρ of the three *n*-alkanes at liquid phase was measured at different temperatures. The results are plotted in Fig. 9 together with the data taken from the literature [57–59]. A gradual decrease of the density of the three *n*-alkanes is observed with the increase of the temperature and the density is higher for the *n*-alkane having a greater number of carbons. A good agreement was observed between the measured and literature data [57–59] (i.e., the maximum registered deviations were 0.20% for C_{16}, 0.05% for C_{18} and 0.25% for C_{20}).

Based on the measured values of λ, c_p and ρ of the three *n*-alkanes in liquid phase, a_T was calculated and the results are given in Table 3 together with the a_T values determined from the hot wire technique and the corresponding deviations. These were found to be less than 17.1% for C_{16}, 31.2% for C_{18} and 29.5% for C_{20}. These high deviations are attributed to the greater uncertainty associated to the calculated a_T values that include both the random and systematic errors of λ, c_p and ρ. In any way, the obtained a_T values by the hot wire technique have less uncertainty and are more accurate.

An important thermal energy storage characteristic of an *n*-alkane is its cumulative thermal energy storage. This is defined as the thermal energy stored in an *n*-alkane by raising its temperature

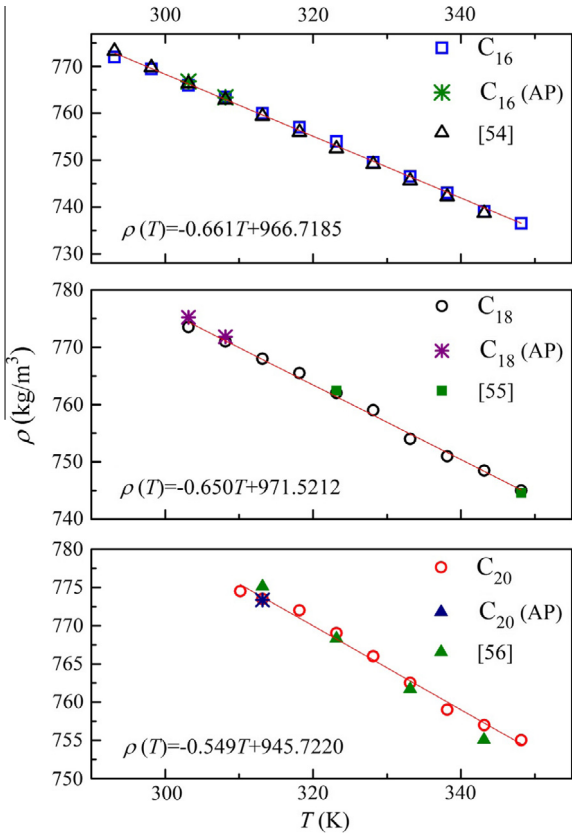

Fig. 9. Density (ρ) of C_{16}, C_{18} and C_{20} as a function of temperature in liquid phase. (AP) are the data measured by Anton Paar densimeter.

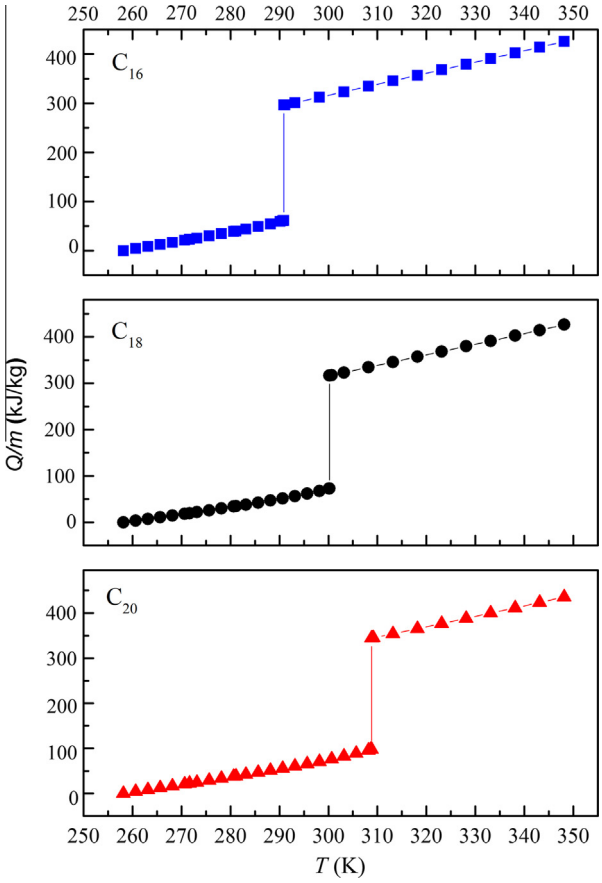

Fig. 10. Variation of the cumulative heat stored in C_{16}, C_{18} and C_{20} as function of temperature.

from a reference temperature to a higher temperature. In this study, the thermal energy stored per unit of mass of the hydrocarbon *n*-alkane (Q/m) was estimated for different heating temperatures up to 348.15 K with a reference temperature of 258.15 K using the following equation:

$$\frac{Q}{m} = \int_{T_1}^{T \leqslant T_m} c_{p,s} dT + \Delta H_m + \int_{T_m \leqslant T}^{T_2} c_{p,l} dT \quad (7)$$

where m is the mass of the *n*-alkane, ΔH_m is its latent heat of melting, T_1 is the initial temperature, T_2 is the final temperature, $c_{p,s}$ and $c_{p,l}$ are the specific heats of solid and liquid *n*-alkane phases, respectively. The first term of the above equation represents the sensible heat of the solid *n*-alkane hydrocarbon phase, the second term is the latent heat of melting, and the third term is the sensible heat of the liquid *n*-alkane hydrocarbon phase.

Fig. 10 shows the cumulative heat stored by each *n*-alkane hydrocarbon as a function of the temperature. As an example, for a temperature of 348.15 K, this is found to be 425.9, 426.3 and 435.4 kJ/kg for C_{16}, C_{18} and C_{20}, respectively. The value of C_{18} is only slightly higher than that of C_{16} due to the lower $c_{p,s}$ values of C_{18} as presented in Fig. 8. It must be pointed out that the sensible heat contribution to the heat stored must be taken into account for any design calculation. For instance, it was observed that the contribution of the latent heat stored increased with the number of carbon in the *n*-alkane hydrocarbon chain (e.g., from 258.15 K to 442.3 K, this contribution is 60.8%, 63.4% and 64.7% for C_{16}, C_{18} and C_{20}, respectively).

4. Conclusions

The thermal properties of the even-numbered *n*-alkanes, *n*-hexadecane (C_{16}), *n*-octadecane (C_{18}) and *n*-eicosane (C_{20}) are measured at different temperatures including both liquid and solid phases and the results were compared with available literature data.

DSC thermograms of C_{16} and C_{18} have a single peak corresponding to melting/crystallization, whereas C_{20} exhibits two almost overlapping crystallization peaks, liquid/solid (i.e., crystallization) and solid/solid transitions (i.e., triclinic structure at lower temperatures than T_r and rotator crystal between T_r and T_m).

A gradual increase of ΔH_m, ΔH_c, T_m, T_c and T_r with increasing the number of carbon atoms of the three *n*-alkanes was observed and the deviations respect to previously reported data were less than 0.8%.

The thermal conductivity (λ) and thermal diffusivity (a_T) of the solid and liquid phases of C_{16}, C_{18} and C_{20} were measured for the first time by the hot wire technique using the same set-up in the temperature range 258–348 K. The obtained values for the liquid phase cannot be in any reliable way extended to the solid phase. High deviations of λ and a_T were detected near the solid/liquid phase transition of the three *n*-alkanes due to the latent heat of melting/crystallization that may affect the temperature of the wire. For the solid phase it is impossible to make any comparison due to the insufficient available data in the literature.

A discontinuity in λ was detected near T_m for each *n*-alkane being λ of the same *n*-alkane in solid state higher than that of the liquid state and the jump of λ near T_m was found to be higher for the *n*-alkane having higher number of carbon atoms. In liquid

phase, λ was higher for the hydrocarbon with more number of carbon atoms and a gradual decrease of λ was observed for C_{16} and C_{20} in all studied temperature range and for C_{18} from its T_m to 333.15 K.

No literature data were found for a_T of the three *n*-alkanes considered in this study. For both liquid C_{16} and C_{20}, very slight decrease was detected for a_T with temperature. However, a slight enhancement of a_T with temperature was observed for C_{18} in liquid phase attributed to the insignificant variation of λ with temperature from 318 to 348 K. Similar to λ in liquid phase up to 330 K, an increase of a_T with the number of carbon atoms of the *n*-alkanes was observed in the temperature range 310–325 K. Moreover, a_T of C_{16}, C_{18} and C_{20} in the solid phase is greater than that of the liquid phase and much dispersions were registered for a_T near the solid/liquid transition temperature.

The cumulative heat stored by each *n*-alkane was estimated as a function of the temperature and it was found an increase of the contribution of the latent heat to the cumulative heat stored with the number of carbon in the *n*-alkane hydrocarbon chain. The cumulative heat stored by C_{18} is slightly higher than that of C_{16} due to the lower $c_{p,s}$ values of C_{18}.

Acknowledgments

The authors gratefully acknowledge the financial support of the UCM-Banco Santader (GR3/14) and the I+D+I Project MAT2010-19249 (Spanish Ministry of Science and Innovation). Partial financial support from *Abengoa Water*, S.L.U. is also acknowledged.

Appendix A. Supplementary material

Supplementary data associated with this article can be found, in the online version, at http://dx.doi.org/10.1016/j.apenergy.2015.01.054.

References

[1] Sharma SD, Sagara K. Latent heat storage materials and systems: a review. Int J Green Energy 2005;2:1–56.
[2] Sharma A, Tyagi VV, Chen CR, Buddhi D. Review on thermal energy storage with phase change materials and applications. Renew Sustain Energy Rev 2009;13:318–45.
[3] Cabeza LF, Castell A, Barreneche C, de Gracia A, Fernández AI. Materials used as PCM in thermal energy storage in buildings: a review. Renew Sustain Energy Rev 2011;15:1675–95.
[4] Zhou D, Zhao CY, Tian Y. Review on thermal energy storage with phase change materials (PCMs) in building applications. Appl Energy 2012;92:593–605.
[5] O'Connor WE, Warzoha R, Weigand R, Fleischer AS, Wemhoff AP. Thermal property prediction and measurement of organic phase change materials in the liquid phase near the melting point. Appl Energy 2014;132:496–506.
[6] Sarı A, Alkan C, Bilgin C. Micro/nano encapsulation of some paraffin eutectic mixtures with poly(methyl methacrylate) shell: preparation, characterization and latent heat thermal energy storage properties. Appl Energy 2014;136:217–27.
[7] Garg HP, Mullick SC, Bhargava AK. Solar thermal energy storage. Holland: Dordrecht; 1985.
[8] Hasnain S. Review on sustainable thermal energy storage technologies, Part I: Heat storage materials and techniques. Energy Convers Manage 1998;39:1127–38.
[9] Farid MM, Khudhair AM, Razack SAK, Al-Hallaj S. A review on phase change energy storage: materials and applications. Energy Convers Manage 2004;45:1597–615.
[10] Regin AF, Solanki SC, Saini JS. Heat transfer characteristics of thermal energy storage system using PCM capsules: a review. Renew Sustain Energy Rev 2008;12:2438–58.
[11] Jegadheeswaran S, Pohekar SD. Performance enhancement in latent heat thermal storage system: a review. Renew Sustain Energy Rev 2009;13:2225–44.
[12] Fan L, Khodadadi JM. Thermal conductivity enhancement of phase change materials for thermal energy storage: a review. Renew Sustain Energy Rev 2011;15:24–46.
[13] Zalba B, Marin JM, Cabeza LF, Mehling H. Review on thermal energy storage with phase change: materials, heat transfer analysis and applications. Appl Therm Eng 2003;23:251–83.
[14] Oró E, de Gracia A, Castell A, Farid MM, Cabeza LF. Review on phase change materials (PCMs) for cold thermal energy storage applications. Appl Energy 2012;99:513–33.
[15] Dimaano MNR, Watanabe T. The capric–lauric acid and pentadecane combination as phase change material for cooling applications. Appl Therm Eng 2002;22:365–77.
[16] Banaszek J, Domanski R, Rebow M, El-Sagier F. Experimental study of solid–liquid phase change in a spiral thermal energy storage unit. Appl Therm Eng 1999;19:1253–77.
[17] Himran S, Suwono A, Mansoori GA. Characterization of alkanes and paraffin waxes for application as phase change energy storage medium. Energy Source 1994;16:117–28.
[18] Eftekhar J, Sheikh AH, Lou DYS. Heat transfer enhancement in a paraffin wax thermal storage system. J Sol Energy Eng 1984;106:299–306.
[19] Karaipekli A, Sarı A, Kaygusuz K. Thermal conductivity improvement of stearic acid using expanded graphite and carbon fiber for energy storage applications. Renewable Energy 2007;32:2201–10.
[20] Martin-Gallego M, Verdejo R, Khayet M, Ortiz de Zárate JM, Essalhi M, López-Manchado MA. Thermal conductivity of carbon nanotubes and graphene in epoxy nanofluids and nanocomposites. Nanoscale Res Lett 2011;6:610.
[21] Fukai J, Hamada Y, Morozumi Y, Miyatake O. Improvement of thermal characteristics of latent heat thermal energy storage units using carbon–fiber brushes: experiments and modeling. Int J Heat Mass Transf 2003;46:4513–25.
[22] http://webbook.nist.gov.
[23] Zou GL, Tan ZC, Lan XZ, Sun LX, Zhang T. Preparation and characterization of microencapsulated hexadecane used for thermal energy storage. Chin Chem Lett 2004;15:729–32.
[24] Genovese A, Amarasinghe G, Glewis M, Mainwaring D, Shanks RA. Crystallisation, melting, recrystallisation and polymorphism of *n*-eicosane for application as a phase change material. Thermochim Acta 2006;443:235–44.
[25] Vargaftik NB. Tables on the thermophysical properties of liquids and gases. 2nd ed. New York: Halsted Press, Division of John Wiley & Sons, Inc.; 1975.
[26] Holmen R, Lamvik M, Melhus O. Measurements of the thermal conductivities of solid and liquid unbranched alkanes in the C_{16}-to-C_{19} range during phase transition. Int J Thermophys 2002;23:27–39.
[27] Vázquez Peñas JR, Ortiz de Zárate JM, Khayet M. Measurement of the thermal conductivity of nanofluids by the multicurrent hot-wire method. J Appl Phys 2008;104:044314.
[28] Ortiz de Zárate JM, Hita JL, Khayet M, Legido JL. Measurement of the thermal conductivity of clays used in pelotherapy by the multi-current hot-wire technique. Appl Clay Sci 2010;50:423–6.
[29] Assael MJ, Charitidou E, Karagiannidis L. The thermal conductivity of *n*-hexadecane + ethanol and *n*-decane + butanol mixtures. Int J Thermophys 1991;12:491–500.
[30] Mukhamedzyanov GKh, Usmanov AGU, Tarzimanov AA. Determinations of the thermal conductivity of liquid saturated hydrocarbons. Izv Vyssh Ucheb Zaved Neft'I Gaz 1963;6:75–9.
[31] Yaws CL. Handbook of thermodynamic and physical properties of chemical compounds. Knovel; 2003.
[32] Wada Y, Nagasaka Y, Nagashima A. Measurements and correlation of the thermal conductivity of liquid *n*-paraffin hydrocarbons and their binary and ternary mixtures. Int J Thermophys 1985;6:251–65.
[33] Bogatov GF, Rastorguev YL, Grigorev BA. Thermal conductivity of normal hydrocarbons at high pressures and temperatures. Chem Technol Fuels Oil+ 1969;5:651–3.
[34] Mustafaev RA. Thermal conductivity of higher saturated *n*-hydrocarbons over wide ranges of temperature and pressure. J Eng Phys Thermophys 1973;24:465–9.
[35] Rastorguev YL, Bogatov GF. Thermal conductivity of *n*-heptadecane and *n*-octadecane at high pressures and temperatures. Chem Technol Fuels Oil+ 1972;8:176–9.
[36] Watanabe H, Seong DJ. The thermal conductivity and thermal diffusivity of liquid *n*-alkanes: C_nH_{2n+2} (n = 5–10) and toluene. Int J Thermophys 2002;23:337–56.
[37] Forsman H, Andersson P. Thermal conductivity at high pressure of solid odd-numbered *n*-alkanes ranging from C_9H_{20} to $C_{19}H_{40}$. J Chem Phys 1984;80:2804.
[38] Duan Q, Tan FL, Leong KC. A numerical study of solidification of *n*-hexadecane based on the enthalpy formulation. J Mater Process Technol 2002;120:249–58.
[39] Stryker PC, Sparrow EM. Application of a spherical thermal conductivity cell to solid *n*-eicosane paraffin. Int J Heat Mass Transf 1990;3:1781–93.
[40] Nabil M, Khodadadi JM. Experimental determination of temperature-dependent thermal conductivity of solid eicosane-based nanostructure-enhanced phase change materials. Int J Heat Mass Transf 2013;67:301–10.
[41] Fang X, Fan LW, Ding Q, Wang X, Yao XL, Hou JF, et al. Increased thermal conductivity of eicosane-based composite phase change materials in the presence of graphene nanoplatelets. Energy Fuel 2013;27:4041–7.
[42] Morikawa J, Hashimoto TH. Simultaneous measurement of heat capacity and thermal diffusivity in solid–solid and solid–liquid phase transitions of *n*-alkane. Thermochim Acta 2000;352–353:291–6.
[43] Miyamoto N, Morikawa J, Hashimoto T. Thermal diffusivity of binary mixture of *n*-tricosane and *n*-tetracosane by Fourier transform temperature wave analysis. Thermochim Acta 2005;431:62–7.

[44] Warzoha RJ, Weigand RM, Fleischer AS. Temperature-dependent thermal properties of a paraffin phase change material embedded with herringbone style graphite nanofibers. Appl Energy 2014.
[45] Ukrainczyk N, Kurajica S, Sipusic J. Thermophysical comparison of five commercial paraffin waxes as latent heat storage materials. Chem Biochem Eng Q 2010;24:129–37.
[46] Khayet M, Ortiz de Zárate JM. Application of the multi-current transient hot-wire technique for absolute measurements of the thermal conductivity of glycols. Int J Thermophys 2005;26:637–46.
[47] Briard AJ, Bouroukba M, Petitjean D, Hubert N, Dirand M. Experimental enthalpy increments from the solid phases to the liquid phase of homologous *n*-alkane series (C_{18}–C_{38} and C_{41}, C_{44}, C_{46}, C_{50}, C_{54}, and C_{60}). J Chem Eng Data 2003;48:497–513.
[48] Xie B, Liu G, Jiang S, Zhao Y, Wang D. Crystallization behaviors of *n*-octadecane in confined space. Crossover of rotator phase from transient to metastable induced by surface freezing. J Phys Chem B 2008;112:13310–5.
[49] González JA, Zawadzki M, Domanska U. Thermodynamics of mixtures containing polycyclic aromatic hydrocarbons. J Mol Liq 2008;143:134–40.
[50] Zhang P, Ma ZW, Wang RZ. An overview of phase change material slurries: MPCS and CHS. Renew Sustain Energy Rev 2010;14:598–614.
[51] Jiang F, Wang X, Wu D. Design and synthesis of magnetic microcapsules based on *n*-eicosane core and Fe_3O_4/SiO_2 hybrid shell for dual-functional phase change materials. Appl Energy 2014;134:456–68.
[52] Parks GS, Moore GE, Renquist ML, Naylor BF, McClaine LA, Fujii PS, et al. Thermal data on organic compounds. XXV. Some heat capacity, entropy and free energy data for nine hydrocarbons of high molecular weight. J Am Chem Soc 1949;71:3386–9.
[53] van Miltenburg JC. Fitting the heat capacity of liquid *n*-alkanes: new measurements of *n*-heptadecane and *n*-octadecane. Thermochim Acta 2000;343:57–62.
[54] Petit JC, Minassian LT. Measurements of $(dv/dt)P$, $(dv/dp)T$, and $(dh/dt)P$ by flux calorimetry. J Chem Thermodyn 1974;6:1139–52.
[55] Dadgostar N, Shaw JM. A predictive correlation for the constant-pressure specific heat capacity of pure and ill-defined liquid hydrocarbons. Fluid Phase Equilibr 2012;313:211–26.
[56] van Miltenburg JC, Oonk HAJ, Metivaud V. Heat capacities and derived thermodynamic functions of *n*-nonadecane and *n*-eicosane between 10 K and 390 K. J Chem Eng Data 1999;44:715–20.
[57] Outcalt S, Laesecke A, Fortin TJ. Density and speed of sound measurements of hexadecane. J Chem Thermodyn 2010;42:700–6.
[58] Caudwell DR, Trusler JPM, Vesovic V, Wakeham WA. The viscosity and density of *n*-dodecane and *n*-octadecane at pressures up to 200 MPa and temperatures up to 473 K. Int J Thermophys 2004;25:1339–52.
[59] Queimada AJ, Marrucho IM, Coutinho JAP, Stenby EH. Viscosity and liquid density of asymmetric *n*-alkane mixtures: measurement and modeling. Int J Thermophys 2005;26:47–61.